Characteristic Life Based Acceleration Transforms for Lead-Free Solder Joint Reliability under Thermal Cycling Conditions

Mudasir Ahmad, Kuo-Chuan Liu
Cisco Systems, Inc.
170 W Tasman Drive,
San Jose, CA 95134
mudasir.ahmad@cisco.com

Abstract

The conversion to Pb-free solders has already been implemented in the consumer market. However, the transition to Pb-free solders in the high performance, mission critical networking/server industry has not yet been fully implemented.

A significant factor in the slow transition to Pb-free solders is the absence of industry accepted Pb-free acceleration transforms that can translate lab test results into field reliability life data. Without such industry accepted acceleration transforms, it is difficult to translate lab test data into reliable predictions of field life performance.

In this two-phase study, a comprehensive set of test data have been generated over a wide spectrum of package types, solder joint metallurgies, joint size, pitch, die sizes, PCB thicknesses and thermal cycling conditions. The effect of aging on acceleration transforms was also included. The data has been analyzed and compared with existing Pb-free and SnPb acceleration transform models.

The data helps explain contradictions in the existing literature, and offers more comprehensive acceleration transforms for Pb-free solders. Some publications indicate that the acceleration transforms for Pb-free solders are the same as SnPb acceleration transforms [1]. Comprehensive results of this study also show that in specific conditions, Pb-free acceleration transforms could even be lower than SnPb acceleration transforms.

Keywords

BGA, Acceleration Factors, Reliability, Solder Joint, Coffin-Manson, Norris-Landzberg, SnPb, Pb-free

Introduction

Pb-free conversion has already taken place for consumer electronics. For high performance networking and computing electronics, the conversion is currently in progress. High performance or mission critical applications require long operating life and much lower failure rates. One of the critical gaps is the lack of a comprehensive, physics-based acceleration transform for BGA packages pervasively used in high performance applications. There have been some recent publications on acceleration transforms, but the data is still limited and there are several unknowns that are yet to be addressed [1-5]. Those unknowns include the effect of aging, ball pitch, solder metallurgy, PCB thickness etc. Several of these unknowns were also present with SnPb assemblies, but because of its pervasive use, there was at least some field data to gage relative performance. One of the challenges with the Pb-free conversion is that the industry has not exactly converged on a single alternative metallurgy. There are several compositions available, and it is unclear what the long term reliability of these variants is. Consequently, it is critical to develop a parametric acceleration transform for at least one metallurgy, which could be used as a baseline.

In this study, a test vehicle was developed to understand several of these unknowns and add to industry knowledge on the behavior of Pb-free acceleration transforms. Several splits and a broad spectrum of package variables were included. The details of the test vehicles, the results, failure analysis and resulting acceleration transforms are the focus of this paper. Also included are comparisons with available industry data and theoretical/numerical estimates.

Test Vehicle Description

To better manage the entire test process, the testing was broken into two phases, but the same components and assembly parameters were used in both phases. The results of Phase 1 have already been published [6]. In paper, the results of Phase 2 are provided, along with overall conclusions from both phases.

The following variables were included in the Phase 1 test vehicle [6]:

Package Variables:

Package type, pitch, die size and metallurgy

PCB Variables:

PCB thickness and copper pad thickness

Test Variables:

Accelerated Thermal Cycling (ATC) conditions (max temp, min temp, delta T) and precondition (aging)

Assembly Variables:

SAC 305 paste and SnPb paste (backward compatible)

The following variables were included in the Phase 2 test vehicle:

Package Variables:

Package type and pitch

Test Variables:

ATC conditions (ramp rate and dwell time)

The details of the packages tested are shown in Table 1 and Table 2. The FCBGA was an organic FCBGA designed specifically to monitor the fatigue life of the flip chip bumps. Consequently, no underfill was dispensed in the final package.

Downloaded from http://meridian.allenpress.com/ism/article-pdf/2010/1/000212/2252782/ism-2010-tp2-paper3.pdf by guest on 14 June 2024

The layout of the daisy chain was such that it went through the least stressed locations on the second level BGA balls. This ensured that the failures in the bumps were captured before the BGAs cracked due to fatigue loading.

The CBGA package was a standard alumina ceramic package, whereas the PBGAs were standard overmolded packages without a heatspreader. The T-BGA packages had tape-based substrates whereas the CABGA package had a standard BT-based substrate.

SN	Package Type	Body Size (mm)	Die Size (mm)	Pitch (mm)	Surface Finish
1	*CBGA	32.5	10.43 x 10.5	1.0	ENiG
2	PBGA1	35	15 x 15	1.0	Ni/Au
3	PBGA2	35	15 x 15	1.0	Ni/Au
4	PBGA3	35	15 x 15	1.0	Ni/Au
5	+PBGA4	35	15 x 15	1.0	Ni/Au
6	*FCBGA	50	17.5 x 17.5	1.0	SOP
7	*T-BGA1	16	7 x 7	0.8	Ni/Au
8	*CABGA	15	7 x 7	0.8	Ni/Au
9	*T-BGA2	9	7 x 7	0.5	Ni/Au
10	T-BGA3	9	4 x 4	0.5	Ni/Au

Table 1: Package Details

SN	Package Type	Solder Metallurgy	Ball Count	Sample Size
1	*CBGA	SAC 305	960	272
2	PBGA1	SAC 105	1156	44
3	PBGA2	SAC 305	1156	56
4	PBGA3	Sn3.5Ag	1156	140
5	+PBGA4	SnPb	1156	140
6	*FCBGA	SAC 305	2377	92
7	*T-BGA1	SAC 305	257	184
8	*CABGA	SAC 305	208	308
9	*T-BGA2	SAC 305	191	184
10	T-BGA3	SAC 305	191	184

Table 2: Package Details

*Samples also used in Phase 2. +Samples used only in Phase 2

Board Design

The test board design used for the test vehicle is shown in Figure 1. The board was designed such that any suspect/failed part could be removed without disrupting the remaining components. Three different board designs were used (details outlined in Table 3).

S/N	Design Variation	Thickness (mils)	Layer Count	Pad Thickness (mils)
1	**Design 1**	93	8	2
2	***Design 2**	125	16	2
3	**Design 3**	125	16	4

Table 3: PCB Details

*Samples also used in Phase 2 for all assembly

The signal layers were designed to have 40% copper mesh whereas the power and ground layers had 70% copper. The surface finish used was OSP, and the PCB was made with phenolic-cured high Tg dielectric.

Sample Size Summary

A summary of all the sample sizes used in the test vehicle is shown in Table 4 and Table 5. For most of the packages, an event detector was used to monitor the nets continuously during temperature cycling. However, for the FCBGA packages where the flip chip bumps were monitored, a data logger was used.

For the parts on which an event detector was used, all the data was stored and for every event, the first recorded failure was manually extracted from the results and recorded as the failure point. This was performed consistently on the nets to ensure that the definition of a failure was the same.

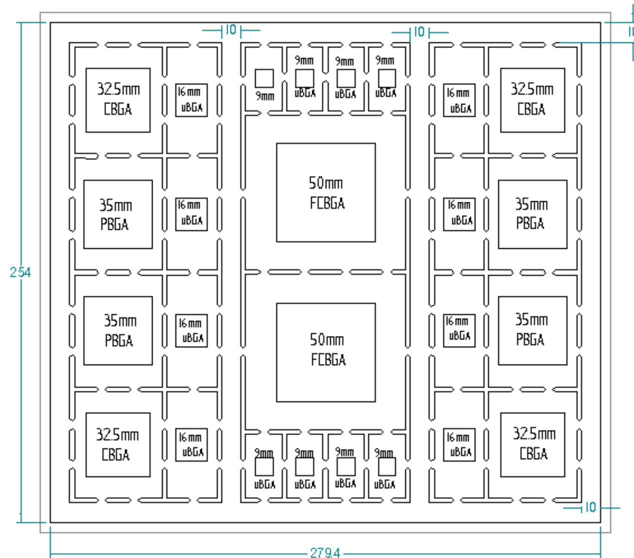

Figure 1: Test Board Design

S/N	Design Variation	Quantities		
1	**Design 1 (93 mils)**	526	432	41
2	**Design 2 (125 mils)**	858	790	60
3	**Design 3 (125 mils, 4 mil pads)**	80	40	4
4	**Design 4 (Mixed Assembly)**	84	84	84
Σ Components		**1548**		
Σ ATC Nets			**1346**	
Σ PCBs				**189**

Table 4: Total Component Quantities (Phase 1)

S/N	Component	ATC 1	ATC 2	ATC 3	ATC 4
1	FCBGA	12	12	12	12
2	CBGA	0	7	7	7
3	CABGA	32	32	32	32
4	T-BGA1	6	6	6	6
5	T-BGA2	0	7	7	7
6	PBGA4	32	32	32	32
Σ Components		82	96	96	96
Σ PCBs		8	8	8	8

Table 5: Total Component Quantities (Phase 2)

Assembly Process

The parts and boards were assembled in a standard convection reflow oven, with SAC305 paste. For the mixed solder splits in Phase 1, SnPb paste was used. Aqueous wash was used in the assembly. Care was taken to ensure that the

Downloaded from http://meridian.allenpress.com/ism/article-pdf/2010/1/000212/2252782/ism-2010-tp2-paper3.pdf by guest on 14 June 2024

peak temperature and time above liquidus on all the parts on the boards were as close to the target as possible.

Coplanarity measurements were performed on the PBGA packages given a history of warpage-induced pillow joints. Parts with coplanarity in excess of 0.006" were not used. Six distinct profiles were developed for the different test splits. Thirty one thermocouple locations were monitored on the assembly during the assembly profile development. The smaller components were closely monitored to ensure that they did not exceed a peak temperature of 260°C. Time zero resistance measurements were performed on all samples to ensure consistent continuity prior to testing.

Test Conditions

In Phase 1, three test conditions were used to derive the acceleration factors (Table 6):

Phase	Test	T_{max} (°C)	T_{min} (°C)	Ramp Rate (°C/min)	Dwell Time (minutes)
1	ATC 1	0	100	10	10
1	ATC 2	25	100	10	10
1	ATC 3	0	75	10	10
2	ATC 1	0	100	10	10
2	ATC 2	0	100	20	10
2	ATC 3	0	100	5	10
2	ATC 4	0	100	10	30

Table 6: Test Conditions for Phase 1 and Phase 2

In addition, some samples were subjected to 100°C, 1000 hours pre-ATC aging in Phase 1. The objective was to understand the impact of aging on characteristic life per package type, and subsequently, acceleration factors. Parts were removed once an open failure was confirmed. The goal of Phase 2 was to incorporate cycling frequency (ramp rate and dwell time) effects.

Test Results

The results of the testing were analyzed and Weibull plots developed for each package type. Rank regression analysis was performed on each split, to ensure that the failure distribution type produced the best fit to the experimental data. Phase 1 results are already published [6], and results of Phase 2 are outlined in this section.

FCBGA (Flip Chip Bumps)

The results of the temperature cycling performed on the FCBGA package are shown in Figure 1.

The results indicate that the characteristic fatigue life of the bumps is in this rank order (lowest to highest): ATC 4 < ATC 3 < ATC 1 < ATC 2. The split with the longest dwell time had the lowest fatigue life, while the split with the longest ramp rate had the highest fatigue life. This indicates that the long dwell time test significantly reduces fatigue life, as compared to the longer ramp time test.

CBGA (SAC305 Ball/SAC305 Paste)

The results of the temperature cycling performed on the CBGA package are shown in Figure 2. While the differences are small, the trends between the three ATC conditions are similar to the FCBGA bumps (ATC4 < ATC3 < ATC2).

The results indicate a reduction in fatigue life due to the longer dwell time during temperature cycling. This is markedly different from the pre-aged case in Phase 1 [6], where aging before temperature cycling actually improved the fatigue life of the package. These results indicate that pre-aging before thermal cycling does not represent conditions that a solder joint undergoes during actual operation, which is more like the long dwell thermal cycling test.

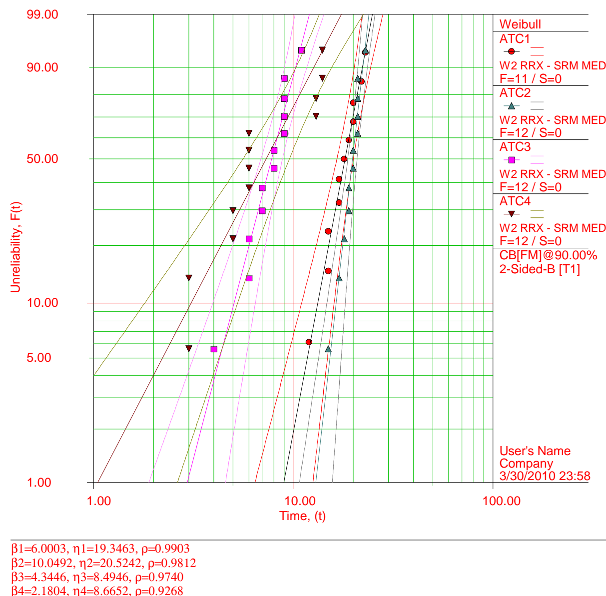

Figure 1: FCBGA (C4) Bump Fatigue Life

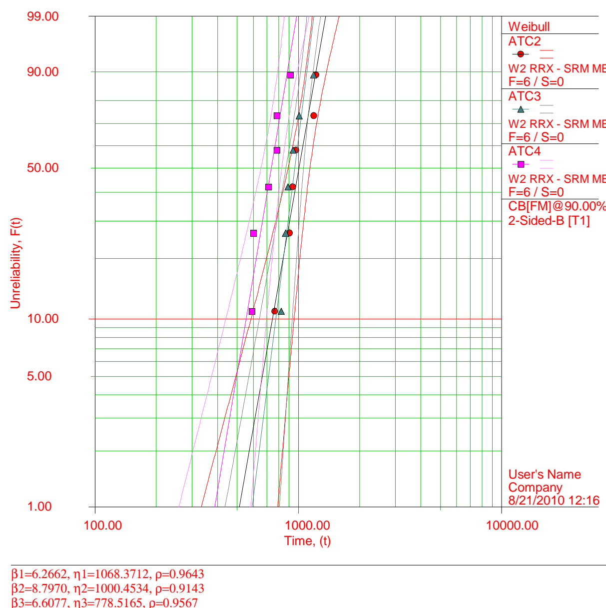

Figure 2: CBGA Fatigue Life

Downloaded from http://meridian.allenpress.com/ism/article-pdf/2010/1/000212/2252782/ism-2010-tp2-paper3.pdf by guest on 14 June 2024

Another interesting observation in comparing the C4 FCBGA data (Figure 1) with the CBGA data (Figure 2) is that the amount of reduction in ATC 4 fatigue life is not the same. There is a higher percentage reduction in fatigue life in the C4 bumps, where the stress levels are higher, as compared to the CBGA balls, where the stress levels are relatively lower.

T-BGA 1 (0.8 mm Pitch)

Figure 3 shows the results of the T-BGA 1 die package

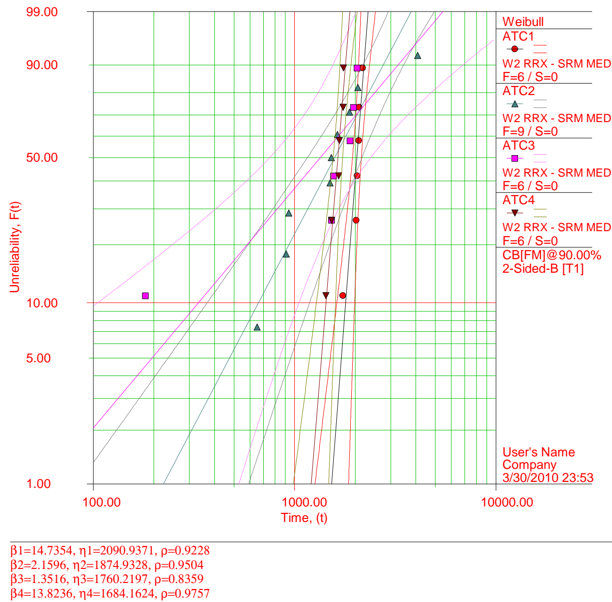

Figure 3: T-BGA 1 (0.8 mm pitch) Fatigue Life

The results of the ATC 4 and 3 splits are not very clear because there weren't enough failures in the data, and there were a few early failures which could not be root caused.

T-BGA 2 (0.5 mm Pitch), Large Die (7 mm)

Figure 4 shows the results of the T-BGA 2 package. The results show the same trends as those for the CBGA and FCBGA packages.

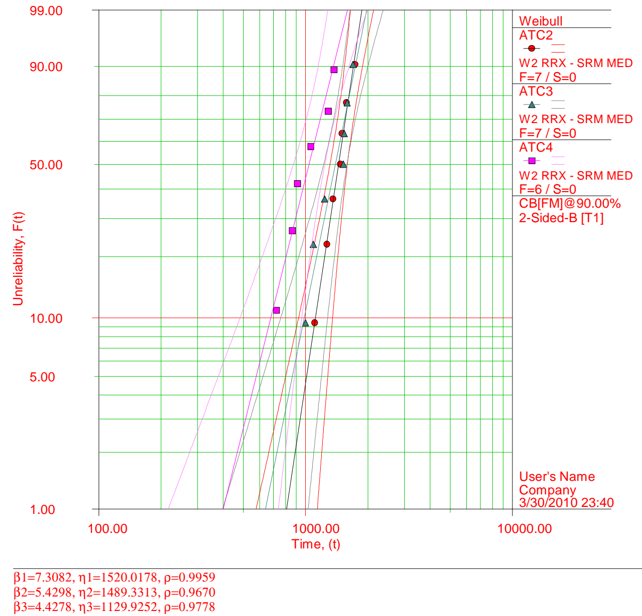

Figure 4: T-BGA 2 (0.5 mm pitch) Fatigue Life

CABGA

Figure 5 shows the results for the CABGA package.

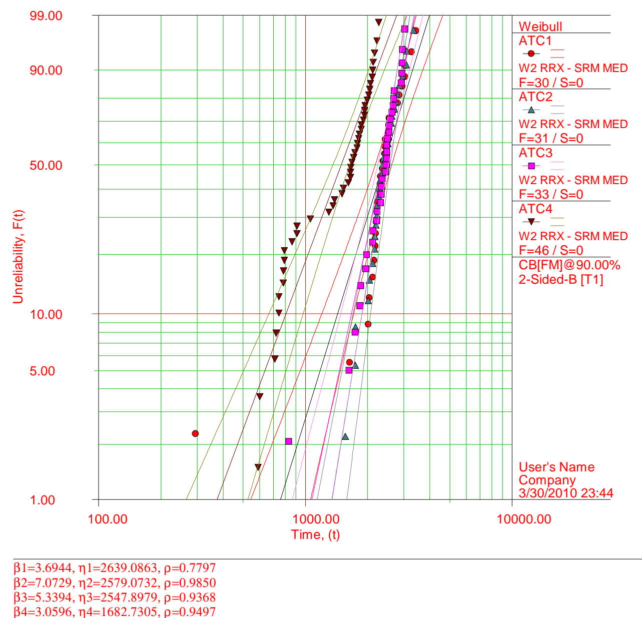

Figure 5: CABGA Fatigue Life

As was observed in the Phase 1 testing [6], there appears to be a bimodal failure distribution in the CABGA package. The bimodal distribution is pronounced in the long dwell split (ATC 4).

The bimodal failure distribution is likely due to the presence of multiple failure locations: under the die edge and at the package corners. Since the daisy chain of the package was not designed to capture both failures independently, the results indicate two different failure rates.

Downloaded from http://meridian.allenpress.com/ism/article-pdf/2010/1/000212/2252782/ism-2010-tp2-paper3.pdf by guest on 14 June 2024

The results indicate that the failure rate of solder joints under the die shadow is markedly different from that under the package corners, and varies depending on the test conditions.

PBGA 4 (35 mm, 1 mm pitch, SnPb Solder/SAC 305 Paste)

Figure 6 shows the results of the PBGA 4 package. This package was included in the testing mix to understand the effects (if any) of using a forward compatible package (SnPb solder balls with SAC 305 paste). The fatigue life of such PBGA packages is notoriously long.

Consequently, not many data points could be collected for each of the test splits. However, for the test splits with enough data points (ATC 1, 2, 4) the trends appear to be similar to those observed for the other packages in the test vehicle.

Failure Analysis

To better understand the underlying basis for the recorded Weibull results, detailed cross-section analysis was performed on several selected assemblies. However, no differences were observed in the cross-sections of the Phase 2 studies when compared to the Phase 1 studies [6]. The failure modes and patterns were the same.

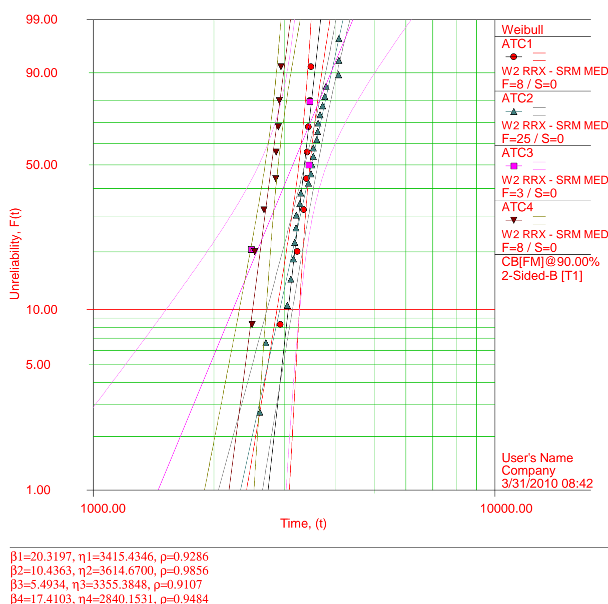

Figure 6: PBGA 4 Fatigue Life

Acceleration Factor Derivation

The most common acceleration factor equation is the Coffin-Manson relationship [8, 9]:

$$N_f \propto \varepsilon_p^c \qquad (1)$$

The Coffin-Manson equation is strictly an empirically derived relationship based on experimentally observed data generated on a wide variety of metals. While several efforts have been made, no fundamental theoretical derivation has been developed of the equation from first principles. Some statistics based relationships have been developed. [10, 11]

A modified form of the Coffin-Manson relationship is the Norris-Landzberg equation:

$$AF = \frac{N_o}{N_t} = \left(\frac{\Delta T_t}{\Delta T_o}\right)^n \left(\frac{f_o}{f_t}\right)^m \exp\left[A\left(\frac{1}{T_{\max,o}} - \frac{1}{T_{\max,t}}\right)\right] \qquad (2)$$

Like the Coffin-Manson relationship, the Norris-Landzberg is a curve-fit derivation of experimentally observed data, based on the premise of the Arrhenius relation for chemical kinetics. As explained in [6], the Norris-Landzberg relation was derived for a specific package construction and material set and does not universally apply to all other package and material sets. Any attempts to generalize the Norris-Landzberg equation have to account for several factors that can impact solder joint reliability: package construction, solder joint shape, height, stress level (due to die, package and PCB) and test/use conditions. It is virtually impossible to come up with an equation that can account for the more than 20 variables that can impact solder joint fatigue life. However, the ultimate metric of solder joint reliability is the *characteristic life* obtained from a standardized test. This characteristic life lends itself to be an all encompassing metric of solder joint reliability and consequently acceleration factors.

The data analysis of Phase 1 and existing literature data indicated a second order relationship between standardized test characteristic life and acceleration factors. [6] The following model was proposed in [6] based on the results of Phase 1:

SN	Characteristic Life (Cycles) in (0-100°C)	n	m	A
1	0-500	0.920	0.25	2030.64
2	500-1500	0.869	0.25	3329.56
3	1500-2000	2.072	0.25	1977.580
4	>2000	1.649	0.25	3109.026

Table 7: Proposed Parametric Acceleration Factor Model

$$AF = \frac{N_o}{N_t} = \left(\frac{\Delta T_t}{\Delta T_o}\right)^n \left(\frac{t_t}{t_o}\right)^m \exp\left[A\left(\frac{1}{T_{\max,o}} - \frac{1}{T_{\min,t}}\right)\right] \qquad (3)$$

Where "*t*" is the lesser of the sum of the hot dwell time and ramp-up-to-hot time or 240 minutes for the thermal cycling profile. [3]

The data from Phase 1 and Phase 2 was combined, rank regression analysis was performed on each fatigue life curve, and the best fitting distribution was used to derive acceleration factors. The characteristic life (62.3%) was used to derive the acceleration factors.

$$AF = \frac{N_o}{N_t} = \left(\frac{\Delta T_t}{\Delta T_o}\right)^{n_1 (N_t)^{n2}} \left(\frac{f_o}{f_t}\right)^{m_1 (N_t)^{m2}} \exp\left[A_1 (N_t)^{A_2}\left(\frac{1}{T_{\max,o}} - \frac{1}{T_{\max,t}}\right)\right] \qquad (4)$$

where

n_1	n_2	m_1	m_2	A_1	A_2
0.6065	0.1296	2.53	-0.358	1415.9	0.1172

Figure 7: Experimentally Derived Acceleration Factors

Downloaded from http://meridian.allenpress.com/ism/article-pdf/2010/1/000212/2252782/ism-2010-tp2-paper3.pdf by guest on 14 June 2024

A comparison between acceleration factors predicted by this model (named "IMAPS10") and the experimental data from Phase 1 and 2 is shown in Figure 8. Also included in Figure 8 are the predictions from the model proposed based on Phase 1 only [6], named "ECTC09".

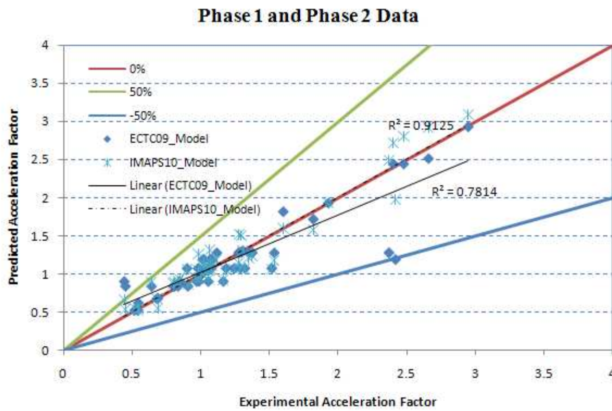

Figure 8: %Error between Predicted and Measured Acceleration Factors (Phase 1 and Phase 2 Combined)

The results show that the linear fit of the model acceleration factors with the IMAPS10 model, which also generalizes the ECTC09 model, are closer to the target line than the linear fit of the ECTC09 model. There is an improvement in accuracy by incorporating frequency effects, while at the same time generalizing the ECTC09 model to make it easier to implement.

The effects of ramp rate and dwell time could be separately incorporated into the model, but that makes the model much more complex and when that model was tested, the results did not yield better accuracy than just the frequency factor model.

It is important to note that the constants (Figure 7) used for this model are based on a standard 0 – 100°C temperature cycling condition. In cases where the lab testing was performed using different temperature cycling conditions, the lab test results will need to be iteratively converted into 0 – 100°C conditions before using this model.

Example 1: if the lab test data is -40 – 125°C, 34 cycles per day, with a characteristic life of 424 cycles. Using Equation 4 and a simple iterative algorithm (can be implemented using goal seek in MS Excel), this lab data equates to 1677 cycles of 0 – 100°C, 36 cycles per day. Equation 4 can now be applied to this equivalent life (1677 cycles) to predict field fatigue life based on the expected field use conditions.

Example 2: let's say we want to use Equation 4 to compare the acceleration factor between two non-standard conditions. Condition 1: -40 – 125°C, 24 cycles per day, characteristic life of 4843 cycles. Condition 2: -55 – 125°C, 48 cycles per day, characteristic life of 3263 cycles. The experimental acceleration factor is 0.674 (4843/3263). Using Equation 4, the equivalent characteristic life for Condition 1 under standard test condition (0-100°C, 36 cycles per day) is iteratively found to be 36,738 cycles. Similarly, the standard equivalent for Condition 2 is 26,776 cycles. So the model predicted acceleration factor is 0.924, which is 37% of the experimental data in this example. This can be represented as:

$$AF_{S-1} = \frac{N_S}{N_1};\ N_1 = \frac{N_S}{AF_{S-1}};\ AF_{S-2} = \frac{N_S}{N_2};\ N_2 = \frac{N_S}{AF_{S-2}}$$

$$AF_{1-2} = \frac{N_1}{N_2} = \frac{N_S}{AF_{S-1}} \times \frac{AF_{S-2}}{N_S} = \frac{AF_{S-2}}{AF_{S-1}} \qquad (5)$$

Where "s" is the standard test condition (0-100°C), while "1" and "2" are the two non-standard test conditions.

Three other published acceleration factor models were applied to the Phase 1 and 2 data, and the results are shown in Figure 11. The results show marginal correlation, and in most cases, no change in predicted acceleration factor for varying experimental acceleration factors. This is because these models don't take into differences in package construction and stresses levels applied to solder joints.

Equation 4 was also applied to a large collection of literature data (Figure 12). The results show very good correlation, within ± 50% with a few outliers. The outliers are inevitable, given the differences in test methods, failure criteria, and another critical factor: As was observed in this test vehicle, the failure rate at different locations within a given BGA footprint can be markedly different. If the daisy chain is not designed to capture different dominating failure modes differently, the results don't capture the failure rates independently, skewing the fatigue life data.

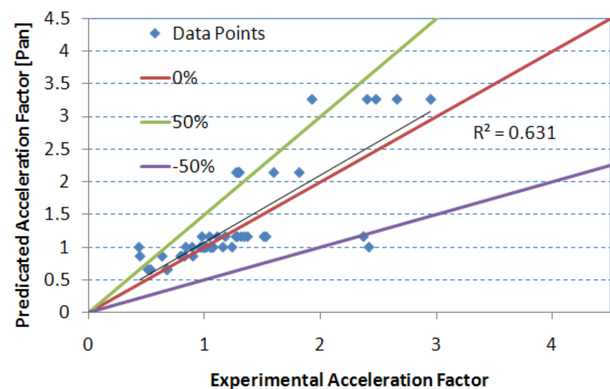

Figure 9: Predicted vs. Experimental AFs using Pan's Model on Phase 1 & 2 Data

Downloaded from http://meridian.allenpress.com/ism/article-pdf/2010/1/000212/2252782/ism-2010-tp2-paper3.pdf by guest on 14 June 2024

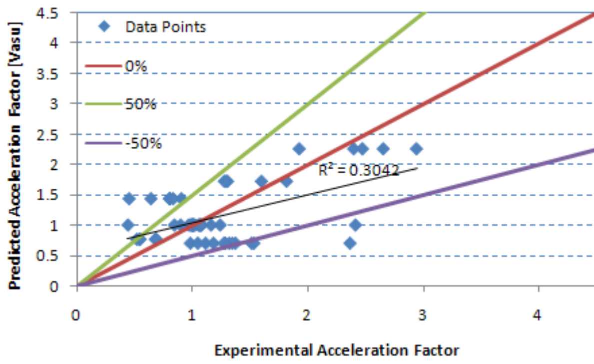

Figure 10: Predicted vs. Experimental AFs using Vasu's Model on Phase 1 & 2 Data

A comparison of some of the other models applied to the same literature data is shown in Figure 13, Figure 14 and Figure 15.

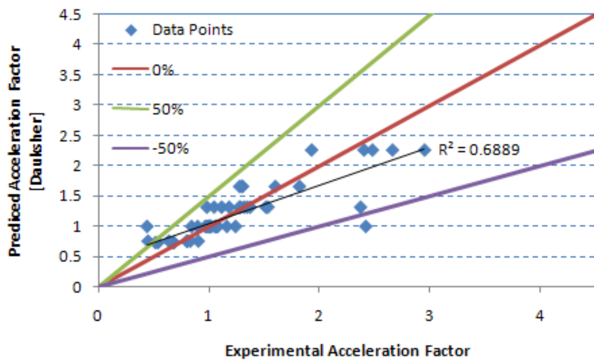

Figure 11: Predicted vs. Experimental AFs using Dauksher's Model on Phase 1 & 2 Data

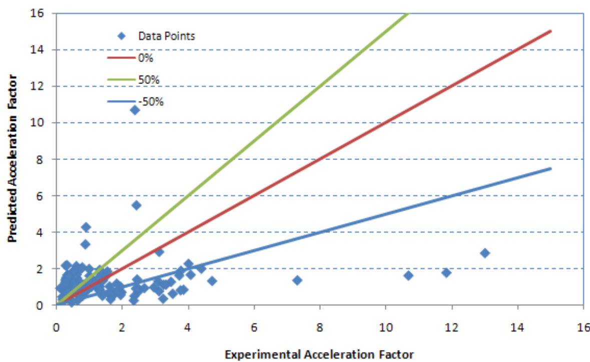

Figure 12: Phase 1&2 Model Applied to Literature Data

The results show that the Pan and Vasu models are not as close to the experimental acceleration factors as the Equation 3 model predictions. The Dauksher model is closeer because it is a curve-fit of most of the data included in this set. However, when the Dauksher model was applied only to the Phase 1 and Phase 2 data, the results weren't as close (Figure 11).

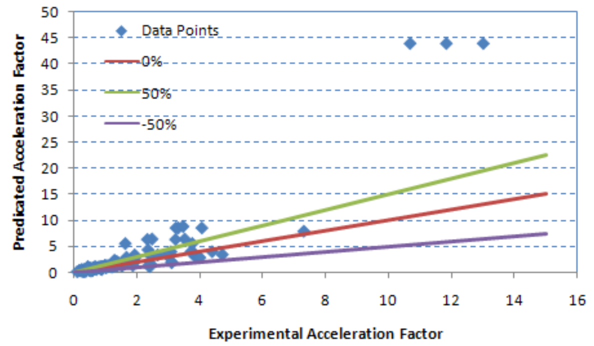

Figure 13: Pan's Model Applied to Literature Data [2]

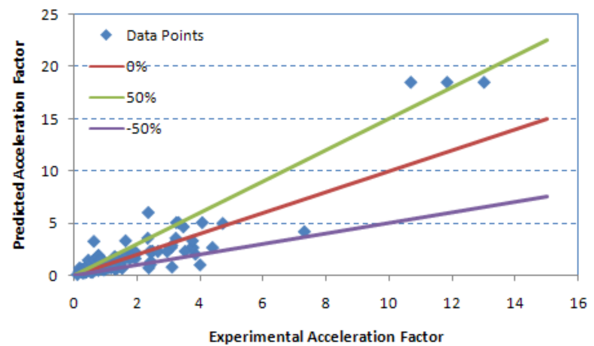

Figure 14: Vasu's Model Applied to Literature Data [1]

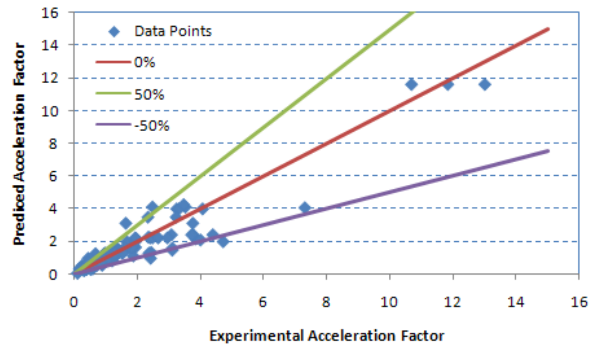

Figure 15: Dauksher's Model Applied to Literature Data [3]

Sensitivity Analysis

Given the second order relationship between characteristic life and acceleration factors, a sensitivity analysis was performed to understand how sensitive the acceleration factor is to T_{max}, T_{min} and Frequency during testing (Figure 16).

The results in Figure 16 show that the acceleration factor is most sensitive to the maximum test temperature, then the minimum test temperature and finally, the frequency of thermal cycling.

The relationship between SnPb and Pb-free acceleration factors and characteristic life for standard test conditions (0-100°C, 10°C/min ramp, 10 minute dwell) is shown in Figure 17. The results indicate that at high stress levels, when the fatigue life is low (<500 cycles), Pb-free solders have lower acceleration factors than SnPb solders.

Downloaded from http://meridian.allenpress.com/ism/article-pdf/2010/1/000212/2252782/ism-2010-tp2-paper3.pdf by guest on 14 June 2024

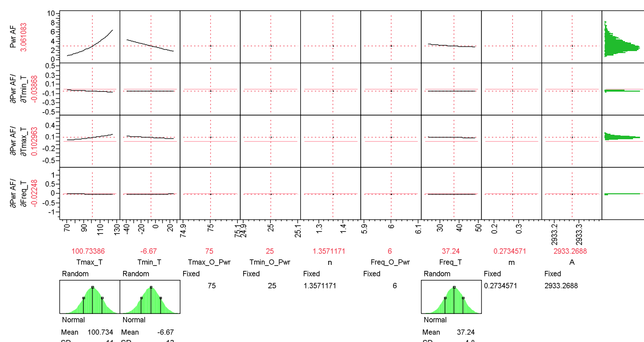

Figure 16: Parametric Sensitivity Analysis

This comparison is based on the assumption that the most accurate acceleration factor for SnPb solders is the Norris-Landzberg equation. It is likely that SnPb solders also exhibit a similar second order dependence on characteristic fatigue life as Pb-free solders, but were not fully articulated in the form of a generalized acceleration factor model.

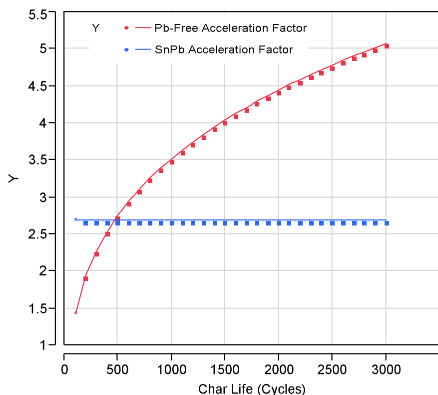

Figure 17: Trend of Acceleration Factors vs. Characteristic Life

Conclusions

A comprehensive test vehicle study to understand the acceleration factors for Pb-free solders is presented. The following specific conclusions can be drawn from the analysis:

1. The effect of solder ball pitch is relatively insignificant in comparison to the overall strain level.
2. Pre-aging at 100°C, 1000 hours does not significantly impact the characteristic life of the solder joints. However, an increased dwell time can reduce characteristic life depending on the package type. Pre-aging cannot necessarily simulate the same fatigue life response as increased dwell time.
3. Die size has an impact on solder joint fatigue life and the resulting acceleration factors.
4. PCB thickness also has an impact on solder joint fatigue life, but depends on the package being tested.
5. Since several design factors (die size, substrate type, PCB thickness etc.) can impact the acceleration factors, the easiest and most representative metric to use for deriving acceleration factor constants is to use the *characteristic fatigue life* under standard test conditions.
6. Norris-Landzberg constants for different ranges of fatigue life under standard 0-100°C temperature cycling have been derived from this study.
7. For BGA footprints where depopulated patterns are used (center and peripheral arrays), independent daisy chain nets should be used to correctly capture the failure modes and failure rates.

Acknowledgments

The authors would like to thank Texas Instruments (Hamid Habibi, Tarak Railkar, Vikas Gupta, Mike Pierce, Darvin Edwards, Kumar Pavuluri, Daryl Heussner and Robin Willhalm), Amkor Technologies (Ahmer Syed and Jinggoy Montenejo), Jabil Circuits Inc. (Peter Verbiest, Hien Ly and Quyen Chu) and Endicott Interconnect Technologies (Susan Donahue, Robert Hartmann, David King and Lee Stradley) for their invaluable support, input and feedback. The feedback and contributions provided by members and management of the Component Quality and Technology Group at Cisco Systems, Inc. are gratefully acknowledged.

References

1. Vasudevan, V., Fan, X., "An Acceleration Model for Lead-Free (SAC) Solder Joint Reliability under Thermal Cycling", *Electronics Components and Technology Conference*, May 2008, pp. 139 - 146.
2. Pan, N., et. al., "An Acceleration Model For Sn-Ag-Cu Solder Joint Reliability Under Various Thermal Cycle Conditions", Surface Mount Technology Association International, 2005.
3. Dauksher, W., "A Second-Level SAC Solder-Joint Fatigue-Life Prediction Methodology", *IEEE Transactions on Device And Materials Reliability*, Vol. 8, No.1, March 2008, pp. 168-173.
4. Salmela, O., "Acceleration Factors for Lead-Free Solder Materials", *IEEE Transactions on Components and Packaging Technologies*, Vol. 30, No. 4, December 2007, pp. 700-707.
5. Zhang, R., Clech, J-P., "Applicability of Various Pb-free Solder Joint Acceleration Factor Models", *SMTAI*, 2006.
6. Ahmad, M., Xie W., Liu KC., Xie J., Towne D., "Parametric Acceleration Transforms for Lead-Free Solder Joint Reliability under Thermal Cycling Conditions", *Electronics Components and Technology Conference*, May 2009, pp. 682 - 691.
7. Ahmad M., Liu K. C., Ramakrishna, G., Xue J., "Impact Of Backwards Compatible Assembly On Bga Thermomechanical Reliability And Mechanical Shock, Pre- And Post-Aging", *SMTAI*, 2008.
8. Norris, K. C., Landzberg, A. H., "Reliability of Controlled Collapse Interconnections," *IBM Journal of Research and Development*, Vol. 13, No. 3, May 1969, pp. 266-271.
9. Ahmad, M., Brillhart, M., "Component to PWB Reliability: Estimating Solder Joint Reliability And The Impact of Lead-Free Solders", Printed Circuits Handbook, Sixth Edition, 2008, pp. 59.12 – 59.13.
10. Sornette, D., Magnin, T., Brechet, Y., "The Physical Origin of the Coffin-Manson Law in Low-Cycle Fatigue", *Europhys. Lett.*, 20 (5)) pp. 433-438, 1992.
11. Huang, J. H., Si, Y., Zheng, L. G., Dong, X. H., "A dislocation model of low-cycle fatigue damage and derivation of the Coffin-Manson equation", *Materials Letters 15*, 212-216, 1992.
12. Kim, D., Ahmad, M., Teng, S., "Reliability Study Of Lead-Free SnAgCu Solder Joints Vs. SnPb Solder Joints In QFN Packages", *SMTAI*, 2006.
13. Bath, J., "Reliability Evaluation Of Lead-Free Snagcu Pbga676 Components Using Tin-Lead And Lead-Free Snagcu Solder Paste", *SMTAI*, 2005.
14. Hall, P. M., Chanchani, R., "Temperature Dependent Thermal Expansion of Materials for Electronic Packages", *Thermal Stress and Strain in Microelectronics Packaging*, New York: Van Nostrand Reinhold, 1993.

Downloaded from http://meridian.allenpress.com/ism/article-pdf/2010/1/000212/2252782/isom-2010-tp2-paper3.pdf by guest on 14 June 2024